General Synthesis of Discrete Mesoporous Carbon Microspheres through a Confined Self-Assembly Process in Inverse Opals

Zhenkun Sun,[†,‡] Yong Liu,[†] Bin Li,[†] Jing Wei,[†] Minghong Wang,[†] Qin Yue,[†] Yonghui Deng,[†] Serge Kaliaguine,[‡] and Dongyuan Zhao[†,*]

[†]Shanghai Key Laboratory of Molecular Catalysis and Innovative Materials, Department of Chemistry and Advanced Materials Laboratory, Fudan University, Shanghai 20043, People's Republic of China and [‡]Département de Génie Chimique, Faculté des Sciences et de Génie, Université Laval, 1065 Avenue de la Médecine, Québec, Canada G1 V 0A6

ABSTRACT A general confined coassembly process has been demonstrated to produce discrete uniform mesoporous carbon microspheres with 0.8−1 μm particle size using 3-D-ordered macroporous silica as the template. The obtained mesoporous carbon microspheres (MC-MSs) have uniform and discrete spherical morphology, variable symmetry (hexagonal *p6mm* or cubic *Im3m*) of mesostructures, high specific surface areas (500−1100 m^2/g), large pore volumes (0.6−2.0 cm^3/g), and highly accessible large mesopores (7−10.3 nm). The particle size of the carbon microspheres can be easily tuned by simply using templates with different macropore sizes. It was found that the smaller MC-MSs (330 nm) with higher surface-to-volume ratio tend to shape into an integral monolithic MC-MS matrix and larger MC-MSs (>800 nm) with lower surface-to-volume ratio to discrete spherical morphology. This feature is attributed to the difference in shrinkage behavior of mesoporous carbon spheres confined in the macropores caused by the interaction between the silica wall and carbon microspheres. Adsorption experiments indicate that the cobalt-based nanoparticle-incorporated mesoporous carbon microspheres exhibit excellent size selectivity for protein adsorption in a complex solution and good magnetic separability for easy recycling.

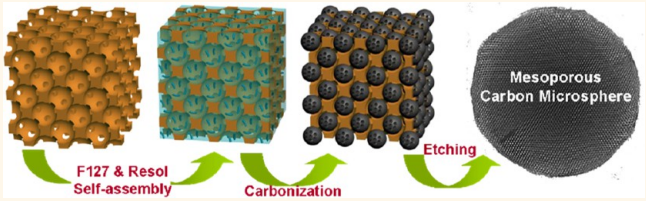

KEYWORDS: confined self-assembly · carbon · microspheres · mesoporous materials · ordered macroporous silica

Microspheres (MS) with well-controlled porosity can provide ready access to a relatively large surface by reducing diffusion lengths compared to their bulk counterparts due to their large surface-to-volume ratio.[1] Particularly, mesoporous microspheres have recently attracted much attention for their large pore size, high surface area, open-framework structures, and unique spherical morphology and their potential applications in the areas of catalysis,[2−4] controlled drug release,[5−9] column packing,[10] and separation.[11] As a kind of advanced carbon nanomaterials, ordered mesoporous carbons have been widely used in various fields due to their uniform and tunable pore size (2.0−50 nm), regularly aligned pore architecture, high surface area (up to 2500 m^2/g), large pore volume, good electrical conductivity, chemical inertness, and hydrophobic property.[12−14] Undoubtedly, the combination of the ordered mesoporous structure and regular spherical morphology to form uniform mesoporous carbon microspheres (MC-MSs) holds a great promise in enhancing their performances and extending their applications. So far, ordered mesoporous silica microspheres have been extensively synthesized through a sol−gel process, and their morphology and porosity can be readily tunable.[15−17] However, it still remains a big challenge to synthesize mesoporous carbon microspheres, especially to precisely control their morphology, internal mesostructure, and porosity.[18,19] Moreover, direct and controllable integration of ordered mesoporous carbons with functional components (*e.g.*, catalytic nanoparticles) has not yet been reported.

* Address correspondence to dyzhao@fudan.edu.cn.

Received for review June 13, 2013 and accepted September 17, 2013.

Published online September 17, 2013
10.1021/nn402994m

Although some efforts have been made to fabricate MC-MSs *via* nanocasting or chemical vapor deposition (CVD), strategies using preformed mesoporous silica microspheres as a hard template, the mesostructure, mesopore, and particle size of final MC-MSs are strongly dependent on the silica templates.[20−23] Combined with the surfactant-templating method, an aerosol-spraying technique was also applied for the synthesis of MC-MSs, but the particle size distribution of obtained microspheres is much wider, resulting in polydispersed particles.[24,25] The suspension-assisted approach has been adopted to synthesize MC-MSs, but it is limited to huge microspheres with particle sizes up to 50 μm.[26] Recently, mesoporous carbons with pore diameters of 30−140 nm have been synthesized through a low-concentration hydrothermal synthesis approach based on the coassembly of Pluronic copolymers and soluble resol and subsequent thermopolymerization. The MC-MSs obtained have small mesopores of 2.0−3.5 nm, which is not favorable for loading biomacromolecules (*e.g.*, proteins) and functional nanoparticles.[27,28] Mesoporous carbons with an appropriate particle size of 1−10 μm and large pore size are crucial for bioimmunology applications, involving large molecule transportation such as protein enrichment, separation, and enzymolysis of biomolecules.[29,30] In addition to the pore size, the control toward the mesostructure of MC-MSs is vital to their application because it directly influences the effective diffusivities of guest molecules.[31,32] Until now, the synthesis of MC-MSs possessing variable mesostructures (different symmetries), tunable particle sizes, and large mesopores (>8 nm) has not been reported.

Herein, we report a general synthesis of discrete mesoporous carbon microspheres with ordered mesopores, variable mesostructures (2-D hexagonal *p6mm* space group or 3-D cubic *Im*$\bar{3}$*m*), tunable particle sizes, and larger mesopores (7−10 nm) compared with conventional mesoporous carbons prepared by the soft-templating process.[12] Furthermore, this general method can make MC-MSs easily functionalized with metal oxides in one step during the generation of carbon microspheres. Such a controllable synthesis was accomplished based on fine-tuning the synthetic parameters of a confined self-assembly process in inverse opals.

RESULTS AND DISCUSSION

Mesoporous Carbon Microsphere Generation. Taking mesoporous carbon microspheres with 2-D hexagonal mesostructure (denoted as MC-MS-1) as an example, the synthetic route is described as the following two steps: First, the monolithic opal structures of polystyrene (PS) spheres (*ca.* 1.1 μm diameter) were replicated inversely with an ethanolic silicate solution to form a silica inverse opal monolith. Then, a confined self-assembly process was accomplished in the voids

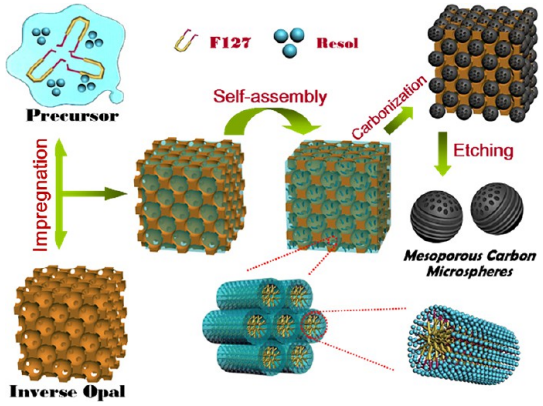

Scheme 1. Formation process of the uniform, discrete, and large-pore-ordered mesoporous carbon microspheres with variable mesostructures using the general confined self-assembly strategy.

of this inverse silica opal monolith with a precursor solution which is normally employed in an evaporation-induced self-assembly (EISA) method for mesoporous carbon synthesis (Scheme 1).[12] This precursor solution consisted of phenolic resol as a carbon precursor and triblock copolymer Pluronic F127 ($EO_{106}PO_{70}EO_{106}$) as a structure-directing agent. A typical precursor was prepared by adding 1.25 g of resols in (20 wt %) ethanolic solution into the mixture containing 0.25 g of F127 and 2.5 g of ethanol. During the self-assembly, the solvent was evaporated completely and the obtained composite was subjected to thermal curing at 100 °C and carbonization at 600 °C in N_2. Then the carbon microspheres were formed *in situ* in the uniform macropores of the silica inverse opals. After a removal of the silica template, monodispersed mesoporous carbon microspheres MC-MS-1 were obtained with discrete spherical morphology.

The as-prepared PS microspheres have a mean diameter of ∼1.1 μm with a standard size deviation of less than 5%, as determined from the SEM images (Supporting Information Figure S1a). The uniformity of size guarantees the ordered alignment of the polymer microspheres during the sedimentation and also the uniform diameter of the final MC-MS products. After a simple sedimentation, the PS microspheres can pack into the highly ordered opal macrostructure which shows colorful sheen (Figure S1a, inset). After the impregnation with the acidic TEOS/ethanol solution and consolidation process, the interstitial voids among the microspheres can be filled by the silica composite, and gel-like species around the polymer microspheres can be visible in the SEM images (Figure S1b and inset); meanwhile, the 3-D-ordered colloidal crystal structure is well-retained. After the calcination in air at 500 °C, the PS microsphere templates are removed, and ordered macroporous structure is obtained with a macropore of ∼1.0 μm and apertures of ∼120 nm (Figure S1c,d). This indicates that the ordered opal structure is faithfully replicated into the inverse macroporous silica. This silica

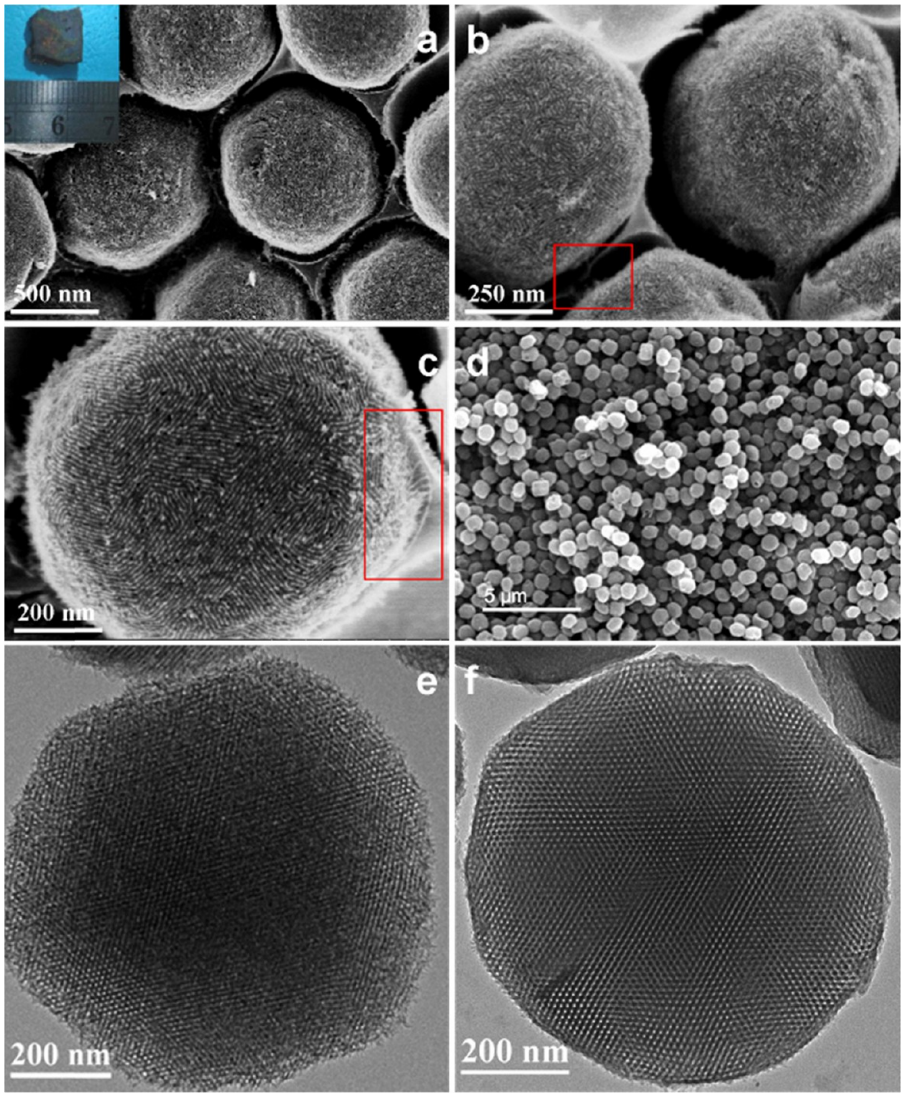

Figure 1. SEM images (a–d) and TEM images (e,f) of the ordered mesoporous carbon microspheres (MC-MSs) prepared by a confined self-assembly method: (a–c) MC-MSs supported in the silica inverse opals before the template removal; (d,e) obtained MC-MSs; (f) TEM image of the crushed MC-MSs. The inset in panel a is the picture of the silica supporting MC-MSs before template removal. Red marked areas in panels b and c indicate the discrete property of MC-MSs and strong affinity between the internal surfaces of macropores for the silica inverse opals and external surface of MC-MSs.

inverse opal can be then used in the confined self-assembly step as a template for the synthesis of MC-MSs. After the casting with F127/resol/ethanol solution, solvent evaporation process, thermal curing, and carbonization at 600 °C, MC-MSs can be *in situ* generated in each macropore of the silica inverse opal (Figure 1a). The obtained silica/carbon monolithic composition is still lustrous, indicating the uniform particle size of the MC-MSs (Figure 1a, inset). It is worth noting that all of the MC-MSs are discrete in individual macropores (Figure 1a–c). Subsequently, the silica template can be removed by HF dissolution. Discrete MC-MSs with a uniform size are left and recovered (Figure 1d and Figure S2a). Numerous ordered stripe-like mesopores can be observed on the surface of MC-MSs, which is attributed to the removal of block copolymer Pluronic F127 (Figure S2a). The diameter of the MC-MSs measured from SEM images is ~810 nm, a little smaller than that of the reverse silica macropores, due to the shrinkage (19%) of the carbon frameworks during the high-temperature carbonization. Nitrogen adsorption–desorption isotherms (Figure S2b) of the sample MC-MS-1 exhibit typical type *I*–*V* curves with a pronounced H2 hysteresis loop and sharp capillary condensation steps which occur at the relative pressure of 0.6–0.8, indicating uniform mesopores. The pore size distribution curve derived from the Barrett–Joyner–Halenda (BJH) model (Figure S2c) further confirms the uniform large mesopore size centered around 8.1 nm. The sample MC-MS-1 has a Brunauer–Emmett–Teller (BET) specific surface area of ~526 m^2/g and a total pore volume of 0.64 cm^3/g. The former is lower than those of the mesoporous carbon powders reported previously; however, the latter is higher than

that for the powders, due to the relatively larger pore size of the MC-MS-1.[12,33] TEM images of the sample MC-MS-1 show a unique hexagonal mesostructure (Figure 1e,f). Since the size of MC-MSs is too large, the particle is milled and crushed before the TEM observations in order to reveal its internal structure (Figure 1f). Then, the highly ordered hexagonal mesopore arrays can be clearly observed at the edge of the crushed particles with an average pore-to-pore distance of ~12.7 nm. According to small-angle X-ray scattering (SAXS) measurements, the MC-MS-1 sample shows a scattering peak at 0.6 nm^{-1} indexed to the 10 reflections of a 2-D hexagonal mesostructure (space group *p6mm*) (Figure S2d), indicating the certain periodicity of the mesostructure with calculated unit cell parameter (*a*) of ~12.5 nm, in agreement with TEM observations. The diameter of MC-MSs can be easily varied to ~1.0 μm just by replacing the starting PS microspheres into ~1.6 μm ones (Figure S3). Compared with 800 nm MC-MSs, the 1 μm ones have stronger shrinkage behavior. That is because the larger carbon spheres have lower surface-to-volume ratio. The surface affinity between internal surface of the silica inverse opals and the external surface of the microspheres cannot prevent the shrinkage effectively.

Tuning toward Mesostructure and Porosity of MC-MSs. In this confined self-assembly process, mesostructures of the carbonaceous spheres can be easily tuned by varying the concentration of Pluronic F127 in the casting precursor. When the weight ratio of F127/resol/ethanol is changed to 1:2:18, the mesoporous carbon microspheres (designated as MC-MS-2) with 3-D cubic mesostructure are obtained. Numerous sphere-like mesopores can be clearly observed from the exposed portion of the spherical particles in SEM images (Figure S4a,b), implying an open pore structure on the surface. The SAXS pattern (Figure S4a, inset) of the sample MC-MS-2 shows a clearly resolved scattering peak at *q* values of ~0.52 nm^{-1} and a weak shoulder peak around 0.92 nm^{-1}. These peaks with the q^2 ratio about 1:3 can be indexed as the 110 and 211 reflections of a body-centered cubic (space group $Im\bar{3}m$) mesostructure. The TEM images (Figure S4e and inset) show that the carbonaceous spheres have a highly ordered mesostructure. N_2 sorption isotherms reveal that the sample MC-MS-2 has a BET surface area and pore volume of ~825 m^2/g and 1.19 cm^3/g, respectively, both higher than the those of the sample MC-MS-1 with 2-D hexagonal mesostructure (Figure S4g). This is probably because the 3-D pore architecture, which has better connectivity than the 2-D one, benefits from the burn-out of exhaust gas from the phenolic resin/F127 composite framework during pyrolysis at 600 °C and the formation of well-developed meso- and microporosity. The mesopore size of the sample MC-MS-2 is around 10.3 nm (Figure S4g, inset).

By slightly modifying and tuning this self-assembly process, the surface area and pore volume of the obtained MC-MSs can be easily enhanced. When 30 wt % of the phenolic resols in the precursor solution is replaced by tetraethoxysilane (TEOS), mesoporous carbon/silica composite microspheres can be formed in macropores of the inverse silica opal template. During the removal of the silica template, the component of the silica in microspheres can be removed at the same time, and the porosity of final MC-MSs (designated as MC-MS-3) can be enhanced. The SEM image shows that the surface of the sample MC-MS-3 becomes more porous and much rougher than those of samples MC-MS-1 and MC-MS-2 (Figure S4c,d). The TEM image (Figure S4f) and SAXS pattern (Figure S4c, inset) clearly reveal that the ordered hexagonal mesostructure is still retained. The sample MC-MS-3 has much higher surface area (1177 m^2/g), pore volume (2.06 cm^3/g), and larger mesopores of ~10.5 nm (Figure S4h and inset). The porosity enhancement is mainly due to the addition of silica species which can increase the mesoporosity after the silica component is etched. Additionally, the introduction of silica species was found to have little influence on the discreteness of the mesoporous carbon microspheres.

Formation Mechanism. When the particle size of MC-MSs decreased to ~330 nm by using silica inverse opal with smaller macropores as a template for the self-assembly process following the same synthesis procedure, only ordered arrays of MC-MSs are generated and no discrete microspheres can be obtained. For comparison, we used the silica inverse opal with a macropore size of ~330 nm and apertures of ~120 nm (the same size of aperture as the previous template) as a template for the synthesis (Figure 2a). After the MC-MS generation, all the microspheres of ~330 nm in diameter (same as macropore size) are located in the silica macropores with the external surface strongly sticking to the internal surface of the inverse opal (Figure 2b,c). It can be seen that MC-MSs are twinborn with neighboring ones with clear symbiotic parts (Figure 2c, the red marked area). After the removal of the template, an integral MC-MS matrix can be obtained (Figure 2d). This MC-MS matrix was subjected to ultrasonic treatment for 5 h to disperse it. Although a few discrete MC-MSs can be found (Figure S5a,b), most of them still aggregate into the matrix (Figure S5c,d). Different from the MC-MSs located in the large macropore (Figure 1a) of silica templates, many hemisphere-like residues of MC-MSs in smaller macropores can be observed from SEM images before removal of silica (Figure 2b,c) because MC-MSs are partially cut down during the sample preparation. This reflects the affinity between internal surfaces of the silica inverse opal, and the external surface of the microspheres largely affects the shrinkage behavior of the carbon particles.

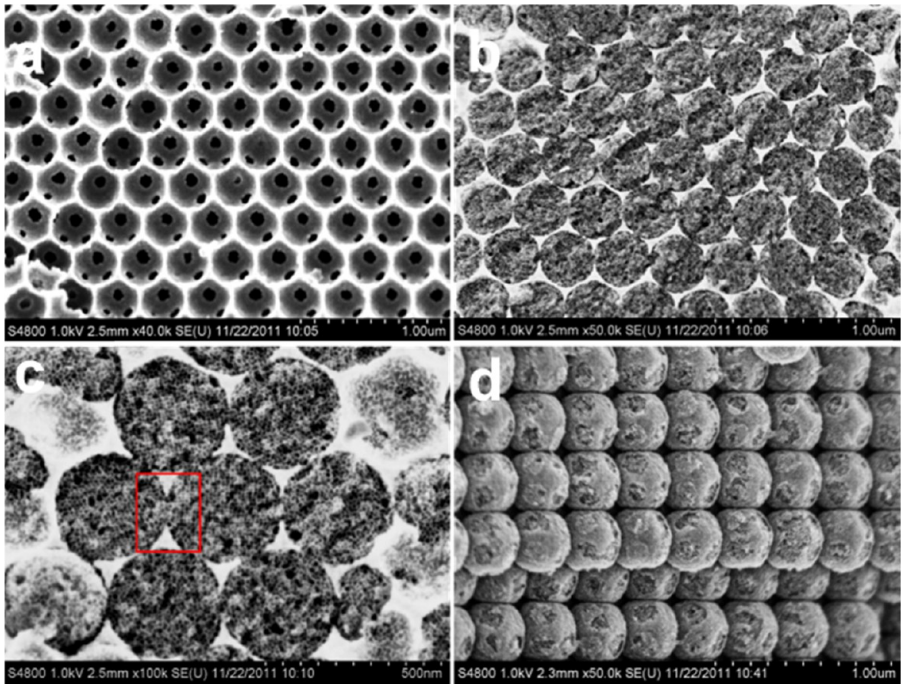

Figure 2. Integral monolithic MC-MS matrixes prepared from the confined self-assembly method by using the silica inverse opal templates with a pore size of ~330 nm: (a) SEM image of the silica inverse opal template; (b,c) SEM images with different magnification of the MC-MS supported in the silica inverse opal before the template removal; (d) SEM image of the obtained MC-MS matrixes. Red marked area in panel c indicates the conjunction of two mesoporous carbon microspheres.

The distinct difference in shrinkage behavior between large and small MC-MSs plays an important role governing the discreteness and mesopore size of the obtained MC-MSs, which is mainly driven by the interface interaction between the internal surface of macropores of the silica inverse opals and the external surface of MC-MSs. Although the resultant large MC-MSs are discrete in the silica template, there is still certain affinity between the internal surfaces of the template and external surface of carbon microspheres. It can prevent the excessive shrinkage of the carbonaceous frameworks of MC-MSs during the thermal curing and carbonization (Figure 1c, the red marked area), resulting in MC-MSs with larger unit cell parameter and mesopore size (~8.1 nm) compared to that for conventional mesoporous carbons.[12] Reversely, such a light shrinkage of the carbonaceous frameworks is still strong enough to prevent the contact between different MC-MSs, resulting in discrete microspheres (Figure 1b, the red marked area). Undoubtedly, the shrinkage of these large MC-MSs, which have low surface-to-volume ratio, is from the outside to the center of the microspheres. When the particle size of MC-MSs decreases, the volume of each particle decreases. During the carbonization, the interaction between the inverse opals and external surface of MC-MSs is firm enough to drastically prevent the volumetric contraction from the outside to the center. Therefore, microspheres bind to each other by the contact area since there is no significant shrinkage of the small MC-MSs, resulting in an integral MC-MS matrix. Compared with larger MC-MSs, the smaller ones have larger pore volume (1.54 cm^3/g) and pore size (12.1 nm), further confirming that the shrinkage of the smaller microspheres is much less than the bigger ones (Figure S6).

Functionalization of MC-MSs with Co-Based NPs. As another important advantage of this strategy, the MC-MSs can be easily functionalized and decorated with metal/metal oxide nanoparticles supported in their frameworks by simply modifying this self-assembly process. Here, 5 wt % of $Co(NO_3)_2 \cdot 6H_2O$ with respect to resol was added as a metal source to the casting precursor when the weight ratio of F127/resols/ethanol in the precursor was 1:1:14. After a similar self-assembly process in the presence of this metal source, ordered MC-MSs supporting Co/Co_xO_y nanoparticles can be synthesized (designated as Co-MC-MS). SEM images show that the Co-MC-MS sample has a uniform spherical appearance of ~820 nm in diameter (Figure S7a). TEM images show the stripe-like and hexagonally arranged pore morphology over large domains, confirming an ordered mesostructure with 2-D hexagonal pore symmetry (Figure 3a and inset). As seen in this TEM image, uniform Co/Co_xO_y nanoparticles are highly dispersed in the carbon matrix with particle sizes of around ~13 nm. N_2 sorption isotherms (Figure S7b) of the sample Co-MC-MS also show representative *I*–*V* curves with pronounced H2 hysteresis loop and large uptake at a low relative pressure due to the existence of well-developed meso- and microporosity. The BET specific surface area and pore volume

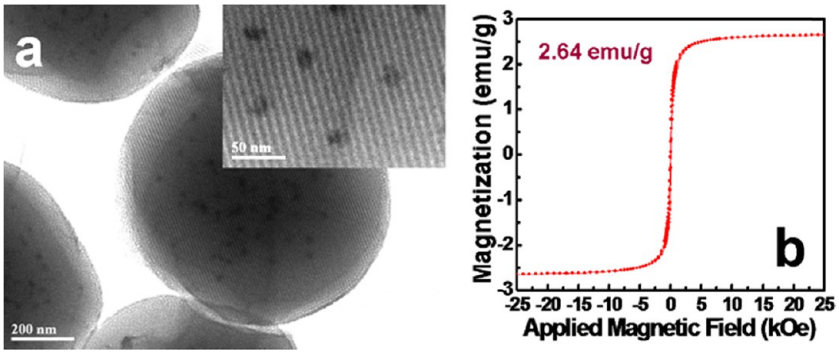

Figure 3. (a) TEM image and (b) magnetic hysteresis loops of the Co-MC-MS sample prepared by the confined self-assembly approach using phenolic resol as a carbon precursor, F127 as a structure-directing agent, and $Co(NO_3)_2 \cdot 6H_2O$ as a metal source. The Co-MC-MS samples have Co_3O_4 content of about 9.6 wt %. The inset in panel a shows a high-resolution TEM image of the sample Co-MC-MS.

are 401 m^2/g and 0.5 cm^3/g, respectively. The mesopore size is around 7.0 nm, slightly lower than that of the sample MC-MS-1 due to the presence of metal oxide nanoparticles (Figure S7b, inset). Thermogravimetric analysis indicates that the Co-MC-MS samples have Co_3O_4 content of about 9.6 wt % (Figure S8a). Wide-angle XRD pattern (Figure S8b) shows that clearly observed diffraction peaks can be assigned to mixed phase of Co_xO_y (Co, CoO, and Co_3O_4). Scanning transmission electron microscopy (STEM) images and corresponding elements mapping further confirm the existence of cobalt-based nanoparticles inside the microspheres (Figure S9). The magnetic properties of the Co-MC-MS composites have a magnetization saturation value of ~2.64 emu/g at 25 000 Oe (Figure 3b). The magnified hysteresis loops further confirm the superparamagnetism of the particles. As a result, the microspheres in their homogeneous aqueous dye-contained dispersion show fast moment to the applied magnetic field and redisperse quickly with a slight shake once the magnetic field is removed (Figure S10). This suggests that the microspheres possess good magnetic responsivity and redispersibility, which is an advantage for their applications as a sorbent. Furthermore, these particles could be easily separated by a hand-held magnet (2000 Oe) from their homogeneous dispersion in 2 min, which suggests the application feasibility of these spheres in separation, adsorption, and so on.

Protein Adsorption. Size-selective adsorption of guest species, which mainly relies on the porous properties of sorbents, is crucial for many applications, especially biomolecule enrichment, separation, detection, and so on.[34−36] Although usual porous sorbents have good capacities and selectivities toward adsorbates, sorbents are difficult to collect and separate from the mixture solution after the adsorption since most of the sorbents are prilled into fine particles and well-dispersed in order to further increase the exposed surface to adsorbates.[37,38] Our Co-MC-MS composites have numerous large mesopores of ~7.0 nm and discrete spherical morphology, which makes them ideal

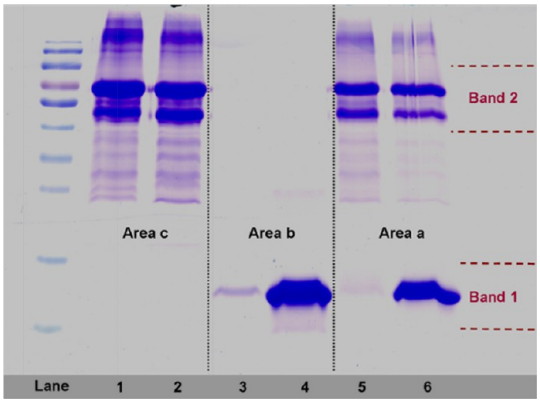

Figure 4. SDS-PAGE analysis results of (area a) the mixture solution containing BSA and Cyt *c*, (area b) Cyt *c* solution, and (area c) BSA solution before (lanes 2, 4, and 6) and after (lanes 1, 3, and 5) the adsorption by the Co-MC-MS samples.

candidates for size-selective adsorption. Furthermore, their good magnetic property is beneficial to effective practical manipulation by magnetic separation. Here, biomacromolecule absorption experiments were performed to study the applicability of the Co-MC-MS materials for size-selective separation of bovine serum albumin (BSA, globular ellipsoid, 5.0 × 7.0 × 7.0 nm) and cytochrome *c* (Cyt *c*, 2.5 × 3.2 × 3.0 nm)[35] in aqueous solution (Figure S11a). After the adsorption, sorbents were collected by a hand-held magnet and supernatant was subjected to sodium dodecyl sulfate polyacrylamide gel electrophoresis (SDS-PAGE) and UV−vis spectrum recording.

The SDS-PAGE analysis (Figure 4) shows two bands in each lane, indicating the adsorption results for BSA (band 2) and Cyt *c* (band 1), respectively. Areas a, b, and c represent the results of mixture solution containing BSA and Cyt *c*, Cyt *c* solution and BSA solution before (lanes 2, 4, and 6) and after (lanes 1, 3, and 5) the adsorption by Co-MC-MS, respectively. It can be seen that, after the adsorption, the width of band 2 in lanes 1 and 5 (areaa a and c) has no significant decrease related to that before shown in lanes 2 and 6. It clearly indicates no significant adsorption on the Co-MC-MS

sample toward BSA neither in BSA solution nor in mixture solution. However, band 1 in lanes 3 and 5 (areas a and b) almost disappears compared with that before the adsorption in lanes 4 and 6, suggesting a much larger adsorption capacity for Cyt *c* either in Cyt *c* solution or in mixture solution. These results suggest that the Co-MC-MS materials with large mesopores of ~7.0 nm can provide access for smaller object Cyt *c* but not for the larger-sized molecule BSA. This implies a good size-selective adsorption. Furthermore, the quantitative analyses using UV−vis spectroscopy show that, toward Cyt *c* molecules, the sample Co-MC-MS has much higher adsorption capacity (~100 mg/g) than that (~4.1 mg/g) toward BSA (Figure S11).[36,39] Such good selectivity and capacity are mainly attributed to their numerous large accessible mesopores and the high surface area. ICP characterization was carried out for the remaining solution after the protein adsorption, and no surplus Co element could be found in it, indicating that cobalt or cobalt oxides did not leach from the carbon scaffolding.

It has been reported that the reaction of hydrogen peroxide with Cyt *c* produces highly reactive ferryl-heme species, which are capable of oxidizing biomolecules and initiating lipid peroxidation.[40,41] In order to demonstrate that Cyt *c* desorbed on the sample Co-MC-MS is still in an active form, the peroxidase activities of Cyt *c* and desorbed Cyt *c* were investigated by using a chromogen, 2,2′-azinobis(3-ethylbenzthiazoline-6-sulfonic acid) (ABTS) as a substrate (Figure S12). ABTS is water-soluble and has a strong absorption at 340 nm. On oxidation, ABTS forms a stable blue-green product presumed to be the cation radical, $ABTS^{+\bullet}$, conveniently followed at λ_{max} of 415 nm.[41] Thus, the increase of the absorbance at 415 nm indicates the peroxidase activity of Cyt *c*. It was found that the enzymatic activity of the desorbed Cyt *c* only decreased slightly compared with its activity before the adsorption on the sample Co-MC-MS (Figure S12), suggesting that the conformation of Cyt *c* was maintained during the adsorption−desorption process. Therefore, we believe that with further carefully designed and engineered surface properties combined with its large mesopores, discrete spherical morphology, and good magnetic property, the novel ordered porous functional material Co-MC-MS can be created as an easily separated sorbent for size-selective absorption and enrichment, which is extremely important for diagnosis, drug delivery, and disease-relevant biomarker screening.

CONCLUSIONS

In summary, we have demonstrated a general confined self-assembly process to create discrete uniform mesoporous carbon microspheres with a particle size of 0.8−1 μm. During this process, carbon microspheres were fabricated *via* a self-assembly process in the micrometer-sized macropores of the silica inverse opal templates. These mesoporous carbon microspheres have uniform and discrete spherical morphology, variable symmetry (hexagonal *p6mm* or cubic $Im\bar{3}m$) mesostructures, high specific surface areas (500−1100 m^2/g), large pore volumes (0.6−2.0 cm^3/g), and large-sized mesopores (7−10.3 nm) which are highly ordered, open, and accessible. The particle size of the carbon microspheres can be easily tuned by simply using templates with different macropore sizes. We found that the smaller MC-MSs (330 nm) with higher surface-to-volume ratio tend to shape into integral monolithic MC-MS matrixes, while larger MC-MSs (>800 nm) with lower surface-to-volume ratio shape into discrete spherical morphology. This discreteness property is mainly controlled by the difference in shrinkage behavior of mesoporous carbon spheres confined in the inverse opals, led by the interaction between the silica template and carbon microspheres. Adsorption experiments indicate that the cobalt-containing mesoporous carbon microspheres exhibit excellent size selectivity for the adsorption in the mixture protein solution of BSA and Cyt *c* and good magnetic responsivity, which makes them easily recovered magnetically. This synthetic strategy is a general and powerful pathway for the functionalization of mesoporous carbon microspheres with embedded metallic nanoparticles and such types of materials hold great potential in biological fields such as diagnosis, drug delivery, and disease-relevant biomarker screening.

MATERIALS AND METHODS

The mesoporous carbon microspheres were prepared through a general confined self-assembly process in silica inverse opal templates. The silica inverse opals were synthesized according to previously reported literature.[29,42,43] An ethanolic precursor solution containing F127 and resol was infiltrated in the macropores of the silica templates. The weight ratio of F127/resol/ethanol was 1:1:14 for the sample MC-MS-1 and 1:2:18 for MC-MS-2. After complete evaporation of ethanol, the templates were taken out from the gel and the excess gel was scraped. Then, the resultant F127/resol/silica composites were subjected to thermal curing at 100 °C for 24 h followed by a carbonization process at 600 °C for 3 h in a N_2 atmosphere. Finally, the MC-MSs were obtained after the silica templates were etched in 10% HF solution for 10 h. For the sample MC-MS-3, 30 wt % of the resol was replaced by TEOS before the confined self-assembly process. The weight ratio of F127/resol/TEOS/ethanol was set to 1:0.7:0.3:13. For the sample Co-MC-MS, 5 wt % of $Co(NO_3)_2 \cdot 6H_2O$ and 4 wt % of acetyl acetone with respect to resol were added to the precursor. The weight ratio of F127/resol/$Co(NO_3)_2 \cdot 6H_2O$/acetyl acetone/ethanol was then 1:1:0.05:0.04:14. Detailed procedures for resol synthesis, PS microspheres, and silica inverse opal preparation and the adsorption tests for proteins can be found in the Supporting Information.

Conflict of Interest: The authors declare no competing financial interest.

Acknowledgment. This work was supported by the State Key 973 Program of the PRC (2012CB224805, 2013CB934104), NSF of China (21073040, 51372041), the Innovation Program of Shanghai Municipal Education Commission (13ZZ004), the Specialized Research Fund for the Doctoral Program of Higher Education of China (20120071110007), the Shanghai Rising Star Project of STCSM (12QH1400300), and Program for New Century Excellent Talents in University (NCET-12-0123).

Supporting Information Available: Detailed procedures of MC-MS fabrication, protein adsorption, and peroxidase activity test of Cyt *c*; detailed characterization (TEM and SEM images, N_2 adsorption desorption isotherms, SAXS patterns, STEM image, and element mapping and wide-angle XRD pattern) of obtained MC-MSs; UV−vis spectra for the protein adsorption process. This material is available free of charge *via* the Internet at http://pubs.acs.org.

REFERENCES AND NOTES

1. Wang, Z.; Li, F.; Stein, A. Direct Synthesis of Shaped Carbon Nanoparticles with Ordered Cubic Mesostructure. *Nano Lett.* **2007**, *7*, 3223–3226.
2. Deng, Y.; Cai, Y.; Sun, Z.; Liu, J.; Liu, C.; Wei, J.; Li, W.; Liu, C.; Wang, Y.; Zhao, D. Multifunctional Mesoporous Composite Microspheres with Well-Designed Nanostructure: A Highly Integrated Catalyst System. *J. Am. Chem. Soc.* **2010**, *132*, 8466–8473.
3. Yu, G.; Sun, B.; Pei, Y.; Xie, S.; Yan, S.; Qiao, M.; Fan, K.; Zhang, X.; Zong, B. Fe_xO_y@C Spheres as an Excellent Catalyst for Fischer−Tropsch Synthesis. *J. Am. Chem. Soc.* **2010**, *132*, 935–937.
4. Ge, J.; Zhang, Q.; Zhang, T.; Yin, Y. Core−Satellite Nanocomposite Catalysts Protected by a Porous Silica Shell: Controllable Reactivity, High Stability, and Magnetic Recyclability. *Angew. Chem., Int. Ed.* **2008**, *47*, 8924–8928.
5. Zhao, Y.; Trewyn, B. G.; Slowing, I. I.; Lin, V. S. Y. Mesoporous Silica Nanoparticle-Based Double Drug Delivery System for Glucose-Responsive Controlled Release of Insulin and Cyclic AMP. *J. Am. Chem. Soc.* **2009**, *131*, 8398–8400.
6. Lee, J. E.; Lee, N.; Kim, H.; Kim, J.; Choi, S. H.; Kim, J. H.; Kim, T.; Song, I. C.; Park, S. P.; Moon, W. K.; *et al.* Uniform Mesoporous Dye-Doped Silica Nanoparticles Decorated with Multiple Magnetite Nanocrystals for Simultaneous Enhanced Magnetic Resonance Imaging, Fluorescence Imaging, and Drug Delivery. *J. Am. Chem. Soc.* **2009**, *132*, 552–557.
7. Kim, J.; Kim, H. S.; Lee, N.; Kim, T.; Kim, H.; Yu, T.; Song, I. C.; Moon, W. K.; Hyeon, T. Multifunctional Uniform Nanoparticles Composed of a Magnetite Nanocrystal Core and a Mesoporous Silica Shell for Magnetic Resonance and Fluorescence Imaging and for Drug Delivery. *Angew. Chem., Int. Ed.* **2008**, *47*, 8438–8441.
8. Zhao, W.; Gu, J.; Zhang, L.; Chen, H.; Shi, J. Fabrication of Uniform Magnetic Nanocomposite Spheres with a Magnetic Core/Mesoporous Silica Shell Structure. *J. Am. Chem. Soc.* **2005**, *127*, 8916–8917.
9. Kim, J.; Lee, J. E.; Lee, J.; Yu, J. H.; Kim, B. C.; An, K.; Hwang, Y.; Shin, C. H.; Park, J. G.; Kim, J.; *et al.* Magnetic Fluorescent Delivery Vehicle Using Uniform Mesoporous Silica Spheres Embedded with Monodisperse Magnetic and Semiconductor Nanocrystals. *J. Am. Chem. Soc.* **2006**, *128*, 688–689.
10. Rebbin, V.; Schmidt, R.; Fröba, M. Spherical Particles of Phenylene-Bridged Periodic Mesoporous Organosilica for High-Performance Liquid Chromatography. *Angew. Chem., Int. Ed.* **2006**, *45*, 5210–5214.
11. Ji, X.; Hampsey, J. E.; Hu, Q.; He, J.; Yang, Z.; Lu, Y. Mesoporous Silica-Reinforced Polymer Nanocomposites. *Chem. Mater.* **2003**, *15*, 3656–3662.
12. Meng, Y.; Gu, D.; Zhang, F.; Shi, Y.; Yang, H.; Li, Z.; Yu, C.; Tu, B.; Zhao, D. Ordered Mesoporous Polymers and Homologous Carbon Frameworks: Amphiphilic Surfactant Templating and Direct Transformation. *Angew. Chem., Int. Ed.* **2005**, *44*, 7053–7059.
13. Schuster, J.; Keilbach, A.; Köhn, R.; Döblinger, M.; Dörfler, T.; Dennenwaldt, T.; Bein, T. Cubic and Hexagonal Mesoporous Carbon in the Pores of Anodic Alumina Membranes. *Chem.—Eur. J.* **2011**, *17*, 9463–9470.
14. Qin, H.; Gao, P.; Wang, F.; Zhao, L.; Zhu, J.; Wang, A.; Zhang, T.; Wu, R. A.; Zou, H. Highly Efficient Extraction of Serum Peptides by Ordered Mesoporous Carbon. *Angew. Chem., Int. Ed.* **2011**, *50*, 12218–12221.
15. Deng, Y.; Qi, D.; Deng, C.; Zhang, X.; Zhao, D. Superparamagnetic High-Magnetization Microspheres with an Fe_3O_4@SiO_2 Core and Perpendicularly Aligned Mesoporous SiO_2 Shell for Removal of Microcystins. *J. Am. Chem. Soc.* **2008**, *130*, 28–29.
16. Zhang, K.; Xu, L. L.; Jiang, J. G.; Calin, N.; Lam, K. F.; Zhang, S. J.; Wu, H. H.; Wu, G. D.; Albela, B.; Bonneviot, L.; *et al.* Facile Large-Scale Synthesis of Monodisperse Mesoporous Silica Nanospheres with Tunable Pore Structure. *J. Am. Chem. Soc.* **2013**, *135*, 2427–2430.
17. Liu, H.; Cui, W.; Jin, L.; Wang, C.; Xia, Y. Preparation of Three-Dimensional Ordered Mesoporous Carbon Sphere Arrays by a Two-Step Templating Route and Their Application for Supercapacitors. *J. Mater. Chem.* **2009**, *19*, 3661–3667.
18. Schuster, J.; He, G.; Mandlmeier, B.; Yim, T.; Lee, K. T.; Bein, T.; Nazar, L. F. Spherical Ordered Mesoporous Carbon Nanoparticles with High Porosity for Lithium-Sulfur Batteries. *Angew. Chem., Int. Ed.* **2012**, *51*, 3591–3595.
19. Mandlmeier, B.; Szeifert, J. M.; Fattakhova-Rohlfing, D.; Amenitsch, H.; Bein, T. Formation of Interpenetrating Hierarchical Titania Structures by Confined Synthesis in Inverse Opal. *J. Am. Chem. Soc.* **2011**, *133*, 17274–17282.
20. Xia, Y.; Yang, Z.; Mokaya, R. Mesostructured Hollow Spheres of Graphitic N-Doped Carbon Nanocast from Spherical Mesoporous Silica. *J. Phys. Chem. B* **2004**, *108*, 19293–19298.
21. Kim, T. W.; Chung, P. W.; Slowing, I. I.; Tsunoda, M.; Yeung, E. S.; Lin, V. S. Y. Structurally Ordered Mesoporous Carbon Nanoparticles as Transmembrane Delivery Vehicle in Human Cancer Cells. *Nano Lett.* **2008**, *8*, 3724–3727.
22. Ren, J.; Ding, J.; Chan, K. Y.; Wang, H. Dual-Porosity Carbon Templated from Monosize Mesoporous Silica Nanoparticles. *Chem. Mater.* **2007**, *19*, 2786–2795.
23. Fuertes, A. B. Template Synthesis of Mesoporous Carbons with a Controlled Particle Size. *J. Mater. Chem.* **2003**, *13*, 3085–3088.
24. Hampsey, J. E.; Hu, Q.; Rice, L.; Pang, J.; Wu, Z.; Lu, Y. A General Approach towards Hierarchical Porous Carbon Particles. *Chem. Commun.* **2005**, *28*, 3606–3608.
25. Yan, Y.; Zhang, F.; Meng, Y.; Tu, B.; Zhao, D. One-Step Synthesis of Ordered Mesoporous Carbonaceous Spheres by an Aerosol-Assisted Self-Assembly. *Chem. Commun.* **2007**, *27*, 2867–2869.
26. Long, D.; Lu, F.; Zhang, R.; Qiao, W.; Zhan, L.; Liang, X.; Ling, L. Suspension Assisted Synthesis of Triblock Copolymer-Templated Ordered Mesoporous Carbon Spheres with Controlled Particle Size. *Chem. Commun.* **2008**, *23*, 2647–2649.
27. Fang, Y.; Gu, D.; Zou, Y.; Wu, Z.; Li, F.; Che, R.; Deng, Y.; Tu, B.; Zhao, D. A Low-Concentration Hydrothermal Synthesis of Biocompatible Ordered Mesoporous Carbon Nanospheres with Tunable and Uniform Size. *Angew. Chem., Int. Ed.* **2010**, *49*, 7987–7991.
28. Li, M.; Xue, J. Ordered Mesoporous Carbon Manoparticles with Well-Controlled Morphologies from Sphere to Rod *via* a Soft-Template Route. *J. Colloid Interface Sci.* **2012**, *337*, 169–175.
29. Sun, Z.; Deng, Y.; Wei, J.; Gu, D.; Tu, B.; Zhao, D. Hierarchically Ordered Macro-/Mesoporous Silica Monolith: Tuning Macropore Entrance Size for Size-Selective Adsorption of Proteins. *Chem. Mater.* **2011**, *23*, 2176–2184.
30. Kim, K. K.; Pack, D. W. Microspheres for Drug Delivery. In *BioMEMS and Biomedical Nanotechnology*; Ferrari, M., Lee, A. P., Lee, L. J., Eds.; Springer: New York, 2006; pp 19−50.
31. Gobin, O. C.; Huang, Q.; Vinh-Thang, H.; Kleitz, F.; Eic, M.; Kaliaguine, S. Mesostructured Silica SBA-16 with Tailored Intrawall Porosity Part 2: Diffusion. *J. Phys. Chem. C* **2007**, *111*, 3059–3065.

32. Menjoge, A. R.; Huang, Q.; Nohair, B.; Eic, M.; Shen, W.; Che, R.; Kaliaguine, S.; Vasenkov, S. Combined Application of Tracer Zero Length Column Technique and Pulsed Field Gradient Nuclear Magnetic Resonance for Studies of Diffusion of Small Sorbate Molecules in Mesoporous Silica SBA-15. *J. Phys. Chem. C* **2010**, *114*, 16298–16308.
33. Lv, Y.; Zhang, F.; Dou, Y.; Zhai, Y.; Wang, J.; Liu, H.; Xia, Y.; Tu, B.; Zhao, D. A Comprehensive Study on KOH Activation of Ordered Mesoporous Carbons and Their Supercapacitor Application. *J. Mater. Chem.* **2012**, *22*, 93–99.
34. Vinu, A.; Murugesan, V.; Tangermann, O.; Hartmann, M. Adsorption of Cytochrome *c* on Mesoporous Molecular Sieves: Influence of pH, Pore Diameter, and Aluminum Incorporation. *Chem. Mater.* **2004**, *16*, 3056–3065.
35. Zhang, M.; Wu, Y.; Feng, X.; He, X.; Chen, L.; Zhang, Y. Fabrication of Mesoporous Silica-Coated CNTs and Application in Size-Selective Protein Separation. *J. Mater. Chem.* **2010**, *20*, 5835–5842.
36. Davis, B. W.; Niamnont, N.; Hare, C. D.; Sukwattanasinitt, M.; Cheng, Q. Nanofibers Doped with Dendritic Fluorophores for Protein Detection. *ACS Appl. Mater. Interfaces* **2010**, *2*, 1798–1803.
37. Mureseanu, M.; Cioatera, N.; Trandafir, I.; Georgescu, I.; Fajula, F.; Galarneau, A. Selective Cu^{2+} Adsorption and Recovery from Contaminated Water Using Mesoporous Hybrid Silica Bio-Adsorbents. *Microporous Mesoporous Mater.* **2011**, *146*, 141–150.
38. Deshpande, P. A.; Polisetti, S.; Madras, G. Rapid Synthesis of Ultrahigh Adsorption Capacity Zirconia by a Solution Combustion Technique. *Langmuir* **2011**, *27*, 3578–3587.
39. Cattoni, D. I.; Kaufman, S. B.; Flecha, F. L. G. Kinetics and Thermodynamics of the Interaction of 1-Anilinonaphthalene-8-sulfonate with Proteins. *Biochim. Biophys. Acta* **2009**, *1794*, 1700–1708.
40. Kim, N.; Jeong, M.; Choi, S.; Kang, J. Peroxidase Activity of Cytochrome C. *Bull. Korean Chem. Soc.* **2004**, *25*, 1889–1892.
41. Radi, R.; Sims, S.; Cassina, A.; Turrens, J. F. Roles of Catalase and Cytochrome *c* in Hydroperoxide-Dependent Lipid Peroxidation and Chemiluminescence in Rat Heart and Kidney Mitochondria. *J. Free Radicals Biol. Med.* **1993**, *15*, 653–659.
42. Li, F.; Wang, Z.; Stein, A. Shaping Mesoporous Silica Nanoparticles by Disassembly of Hierarchically Porous Structures. *Angew. Chem., Int. Ed.* **2007**, *46*, 1885–1888.
43. Schroden, R. C.; Al-Daous, M.; Stein, A. Self-Modification of Spontaneous Emission by Inverse Opal Silica Photonic Crystals. *Chem. Mater.* **2001**, *13*, 2945–2950.